Supplementary Information

Nitrogen-Induced Deep Reconstruction and Formation High-Valent Nickel Species γ-NiOOH Surface Layer on $NiFe_{alloy}$/NiFeN Pre-catalysts for the Efficient Water Oxidation

Gouda Helal,‡[abc] Zhenhang Xu,[b] Wei Zuo,‡[b] Jun Qian,[a] Gongzhen Cheng *[b] and Pingping Zhao*[a]

Computational methods

DFT calculations were performed by using the Vienna Ab-initio Simulation Package (VASP). The exchange–correlation interactions were described by generalized gradient approximation (GGA) with the Perdew–Burke–Ernzerhof (PBE) functional. Spin-polarization was included in all the calculations and a damped van der Waals correction was incorporated using Grimme's scheme to better describe the non-bonding interactions. A plane wave cut-off energy of 500 eV was used, and a 3×3×1 Monkhorst-Pack grid k-points was employed. The residual force and energy on each atom during structure relaxation were converged to 0.005 eV $Å^{-1}$ and 10^{-5} eV, respectively. To account for the effect of localized d electrons of Ni and Fe ions, a Hubbard U correction was introduced with U values of 6.4 and 4.2 eV, respectively. The OER pathway was described as the adsorption of successive intermediate species on the catalyst and the relevant reaction energies were as follows (*Eq.* 1 ~ *Eq.* 4):

1. $OH^- + cat \rightarrow *OH\text{-}cat + e^-$
2. $*OH\text{-}cat + OH^- \rightarrow *O\text{-}cat + H_2O + e^-$
3. $*O\text{-}cat + OH^- \rightarrow *OOH\text{-}cat + e^-$
4. $*OOH\text{-}cat + OH^- \rightarrow O_2\uparrow + H_2O + e^-$

The ''cat" represented the active site when OER occurred. The ''*OH", ''*O", ''*OOH" represented the intermediate species adsorbed on the active sites. In order to evaluate OER activity, we calculated the free energy (ΔG_1 ~ΔG_4) using the computational standard hydrogen electrode model. The free energy calculation could be obtained as follows:

$\Delta G_1 = G_{OH\text{-}cat} - G_{cat} - G_{H2O} + 1/2G_{H2} - eU + K_BTLn10 \cdot pH$

$\Delta G_2 = G_{O\text{-}cat} - G_{OH\text{-}cat} + 1/2G_{H2} - eU + K_BTLn10 \cdot pH$

$\Delta G_3 = G_{OOH\text{-}cat} - G_{O\text{-}cat} - G_{H2O} + 1/2G_{H2} - eU + K_BTLn10 \cdot pH$

$\Delta G_4 = 4.92 - \Delta G_1 - \Delta G_2 - \Delta G_3$

It should be noted that -eU represented the free energy changes for one electron transfer where U was electrode potential respect to the standard hydrogen electrode. For pH ≠ 0, pH effected on free energy could be defined as $-K_BTLn10 \cdot pH$, where K_B

was Boltzman constant. ΔG_4 was calculated by 4.92 - ΔG_1 - ΔG_2 - ΔG_3 to avoid calculating the O_2 adsorption and desorption. It was known that the DFT calculation might not accurately describe the free energy of O_2 molecule in the gas phase and hence we used H_2O and H_2 as reference and from there we extracted the free energy of O_2 through the reaction $O_2 + 4(H^+ + e^-) \rightarrow 2H_2O$. The equilibrium potential for this reaction was 1.23 V and since it was a four electron transfer reaction, the full energy was 4 × 1.23 = 4.92 eV. This analysis was based on the scheme developed by Norskov's group. The overpotential of OER in this mechanism was defined as η_{OER} = max(ΔG_{OER}/e) - 1.23 V.

Supplementary Images characterization:

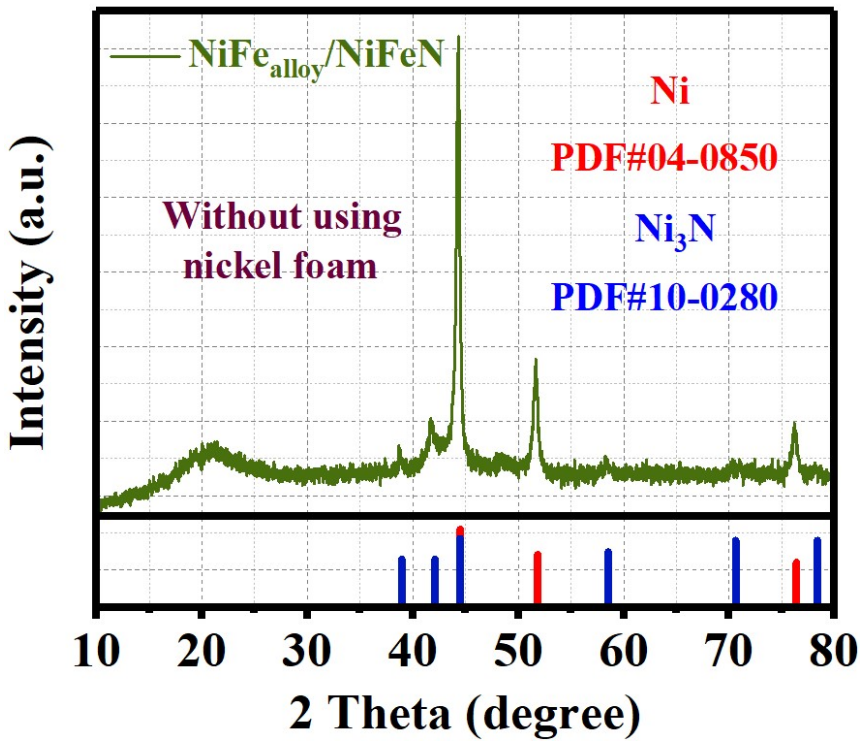

Figure S1. XRD pattern of $NiFe_{alloy}$/NiFeN prepared without using Ni foam.

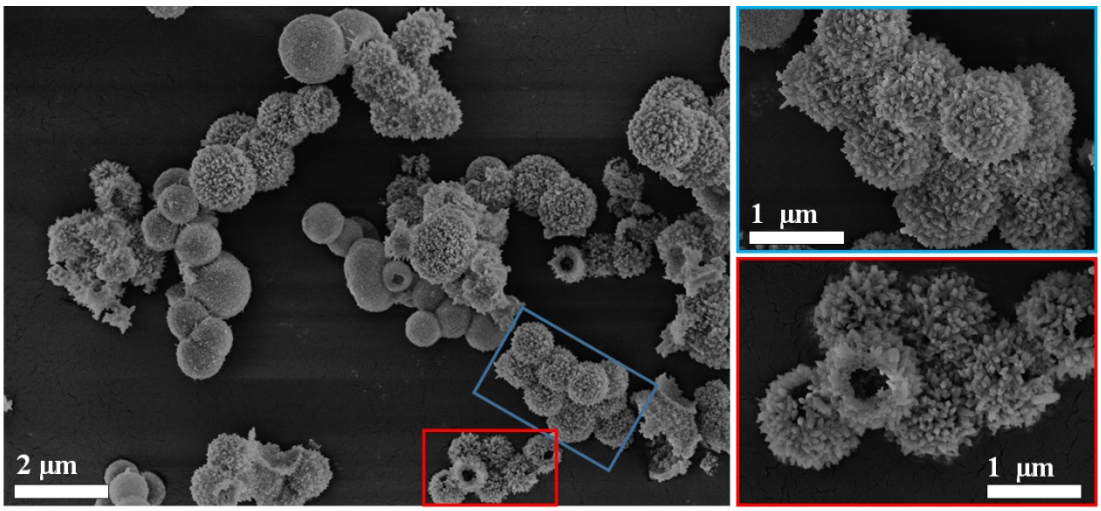

Figure S2. SEM images of Ni MOF.

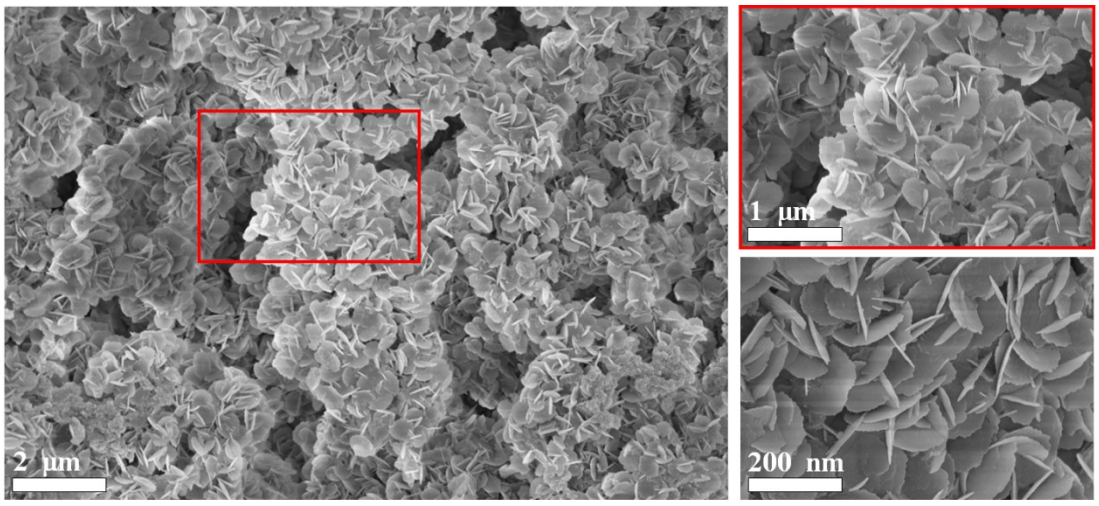

Figure S3. SEM images of NiFeLDH.

).

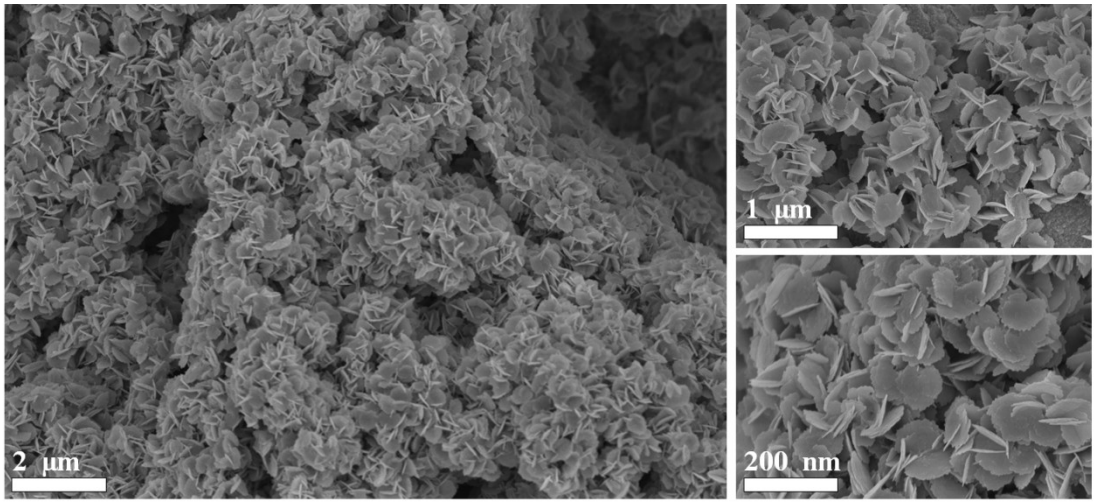

Figure S4. SEM images of NiFeO.

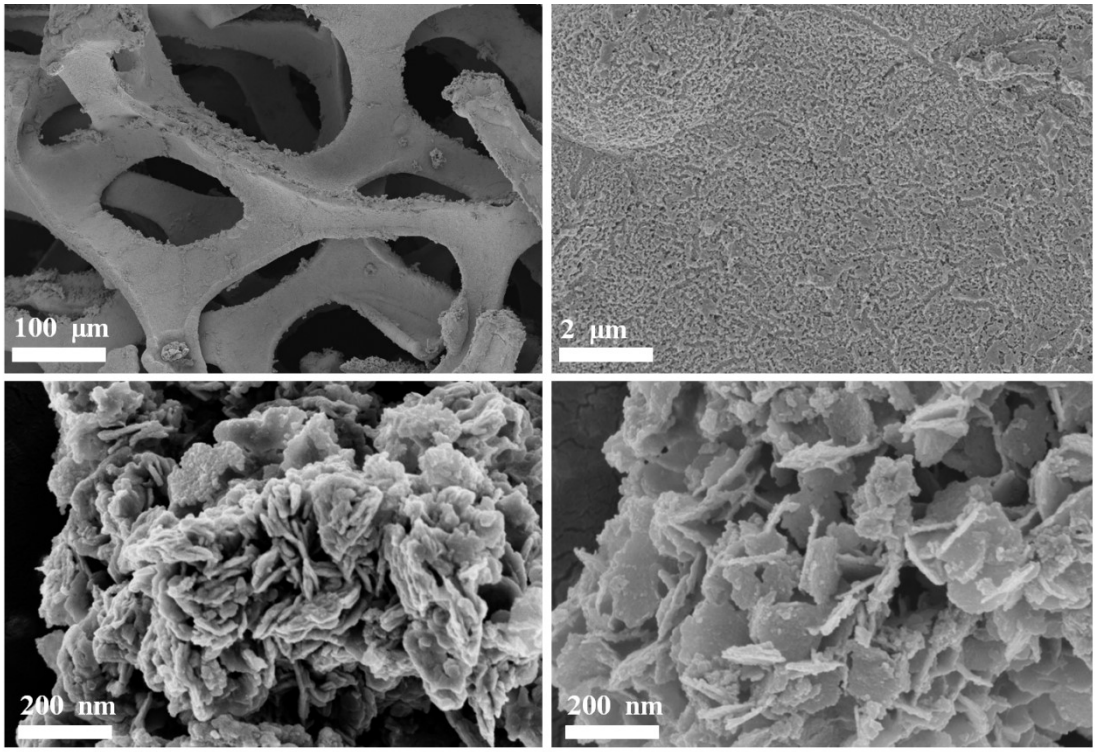

Figure S5. SEM images of $NiFe_{alloy}$/NiFeN.

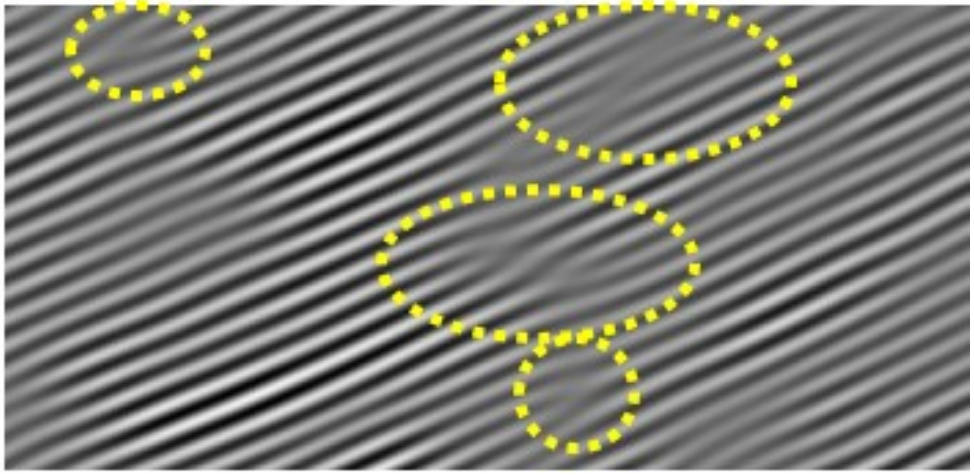

Figure S6. Atomic lattice image reveal numerous stacking faults and dislocations in the $NiFe_{alloy}$/NiFeN heterostructure.

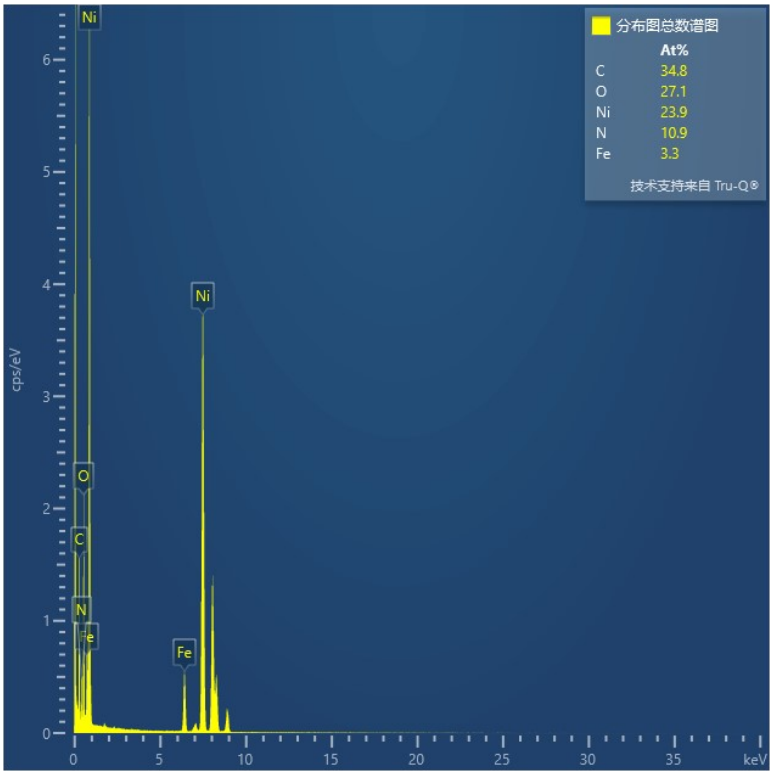

Figure S7. Elemental EDX of $NiFe_{alloy}$/NiFeN heterostructure.

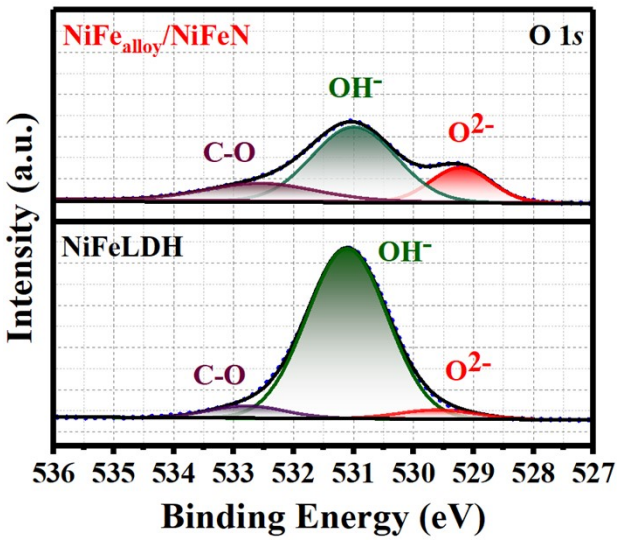

Figure S8. High resolution O 1*s* XPS profile of NiFe$_{alloy}$/NiFeN heterostructure and NiFeLDH before OER.

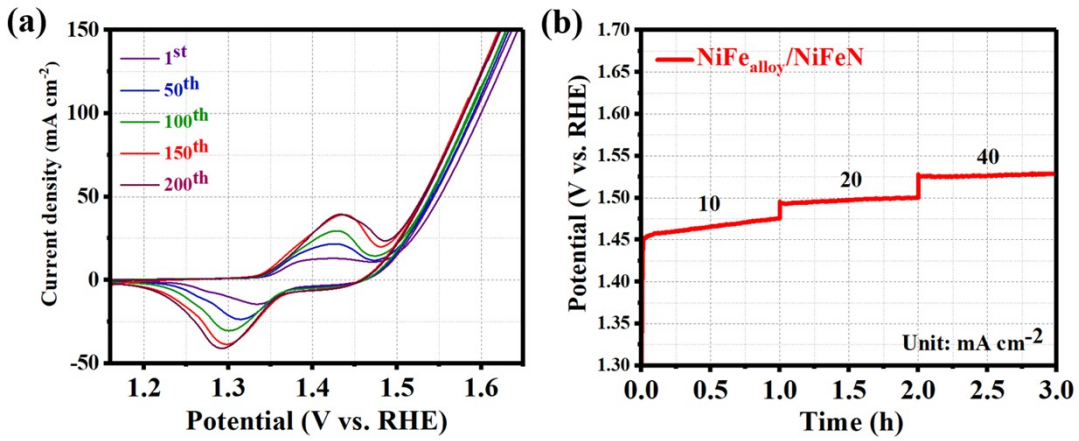

Figure S9. a) The steady state performance of NiFe$_{alloy}$/NiFeN after multiple CV at very low scan rate (5 mV s^{-1}) and b) Potential behavior using controlled current densities.

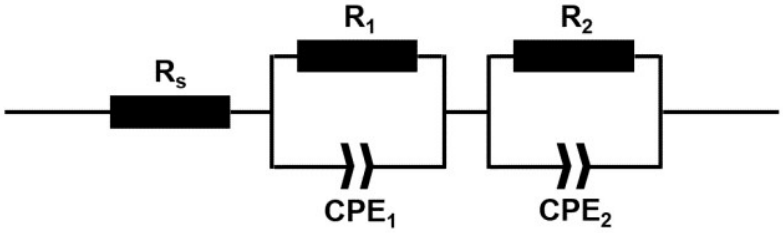

Figure S10. Equivalent circuit used for the fitting of the EIS, where R_s, R_1, R_2, CPE_1, and CPE_2 represent the solution resistance, electrode texture, charge transfer resistances and constant phase elements, respectively.

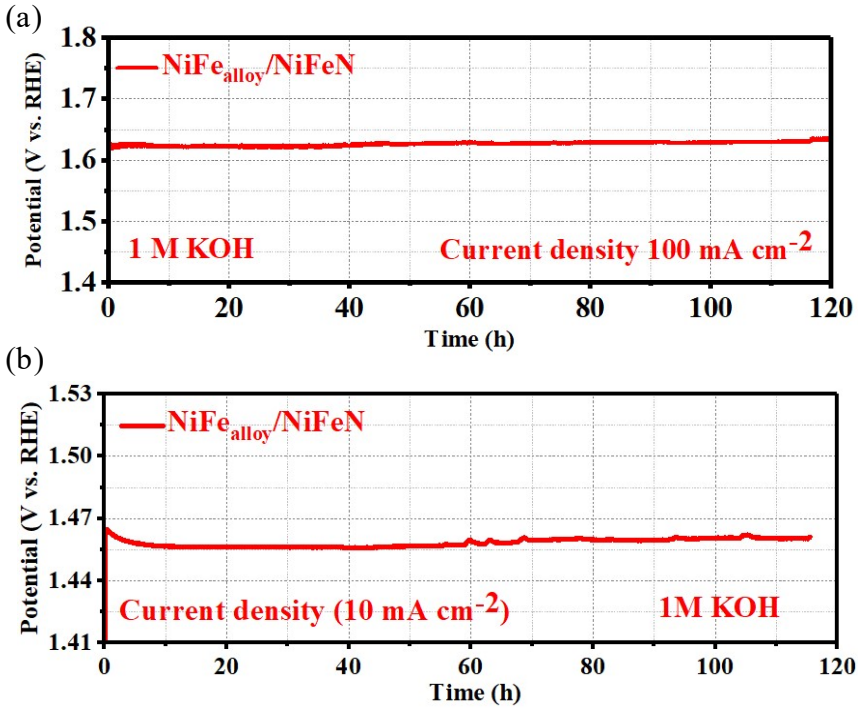

Figure S11. Long-term durability test of $NiFe_{alloy}$/NiFeN at current density: a) 100 mA cm^{-2} and b) 10 mA cm^{-2}.

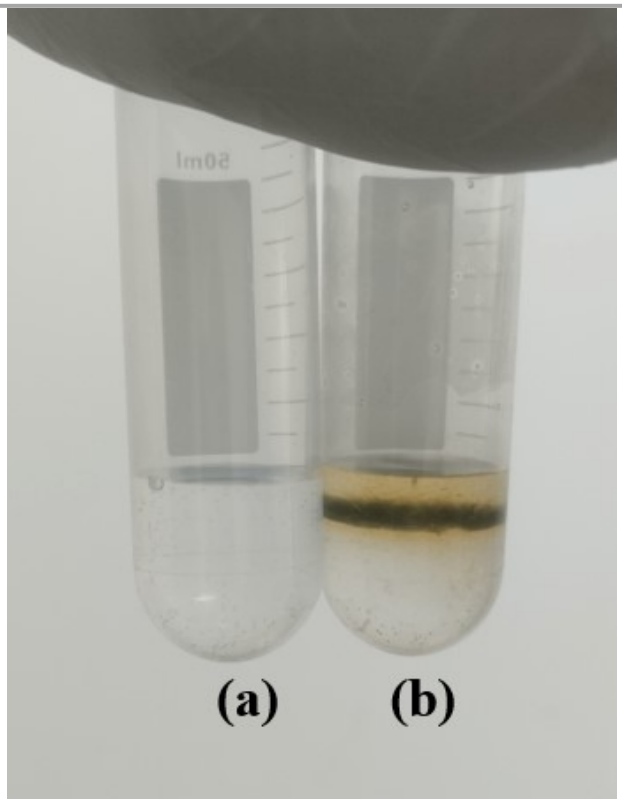

Figure S12. Brown ring test of the electrolyte: a) Before long term durability; and b) After long term durability.

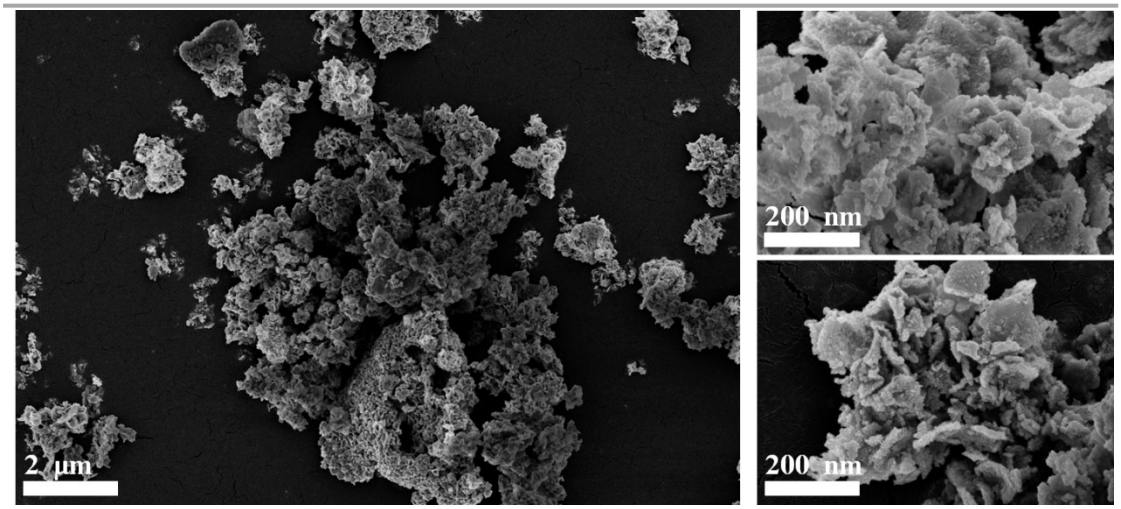

Figure S13. SEM images of $NiFe_{alloy}$/NiFeN after OER.

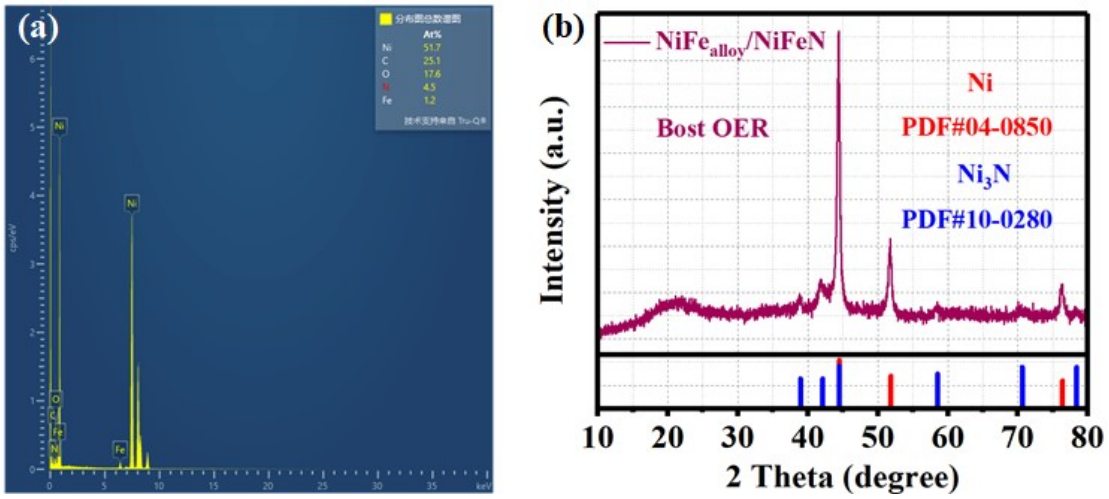

Figure S14. a) EDX after OER, and b) XRD pattern of $NiFe_{alloy}$/NiFeN after OER.

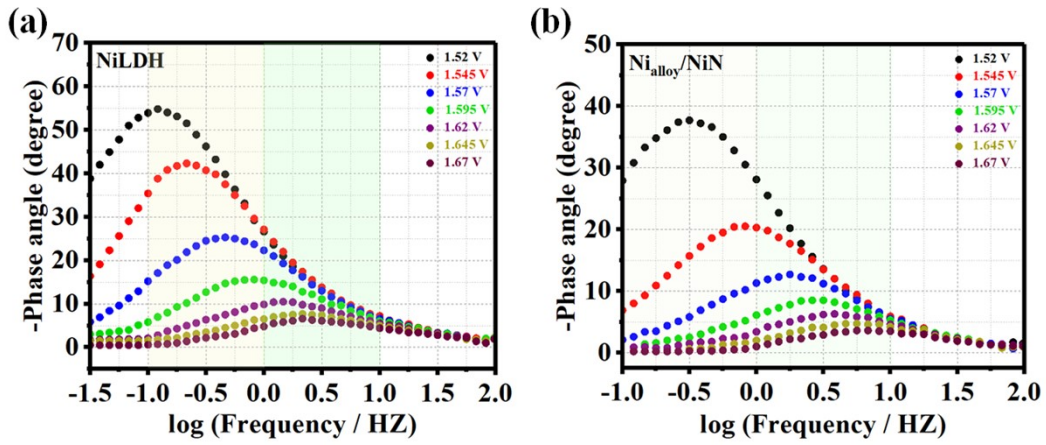

Figure S15. Bode plots: a) NiLDH and b) Ni_{alloy}/NiN at potential range from 1.52 to 1.67 V (vs RHE).

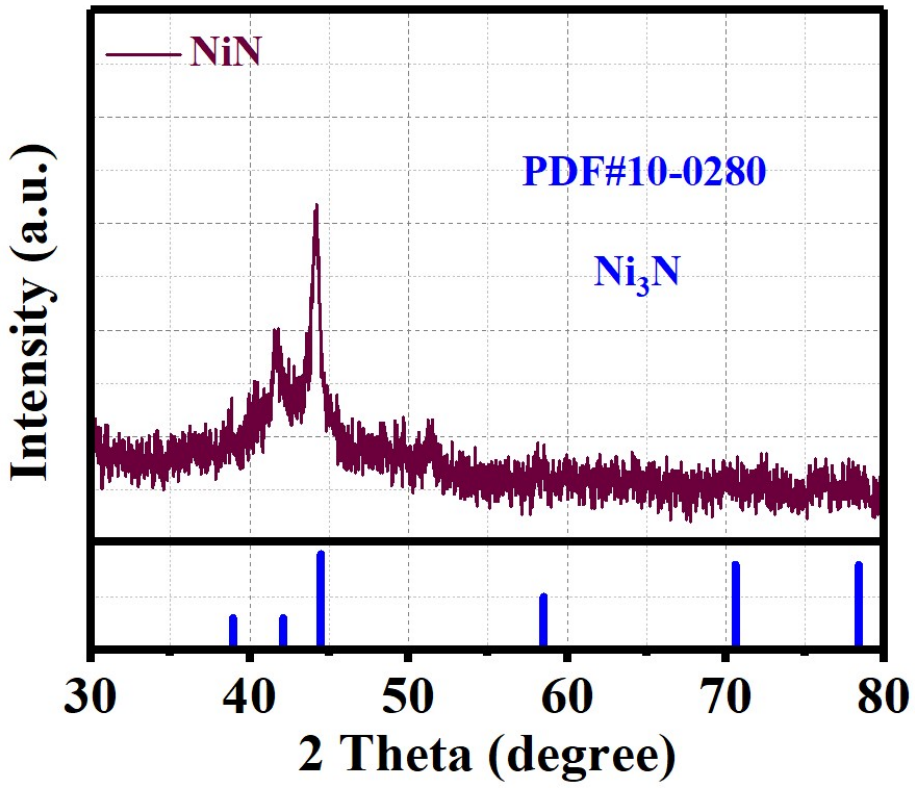

Figure S16. XRD pattern of NiN prepared based on Ni MOF precursor.

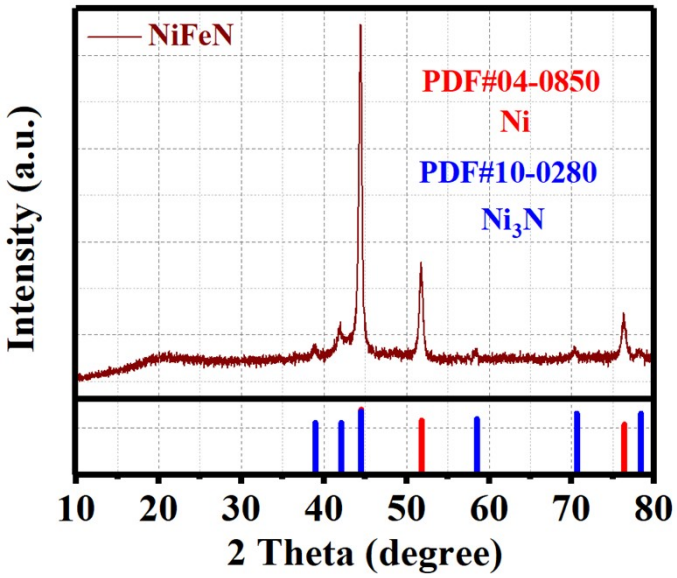

Figure S17. XRD pattern of NiFeN prepared based on NiFeO precursor.

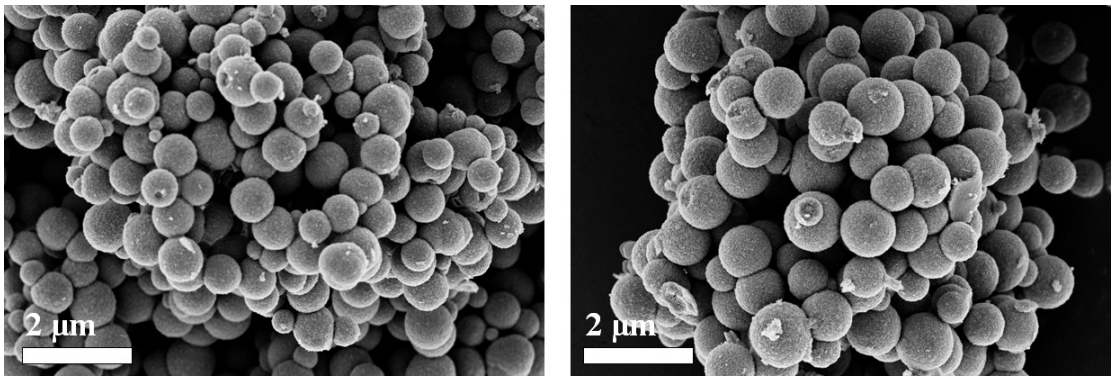

Figure S18. SEM images of NiN prepared based on Ni MOF precursor.

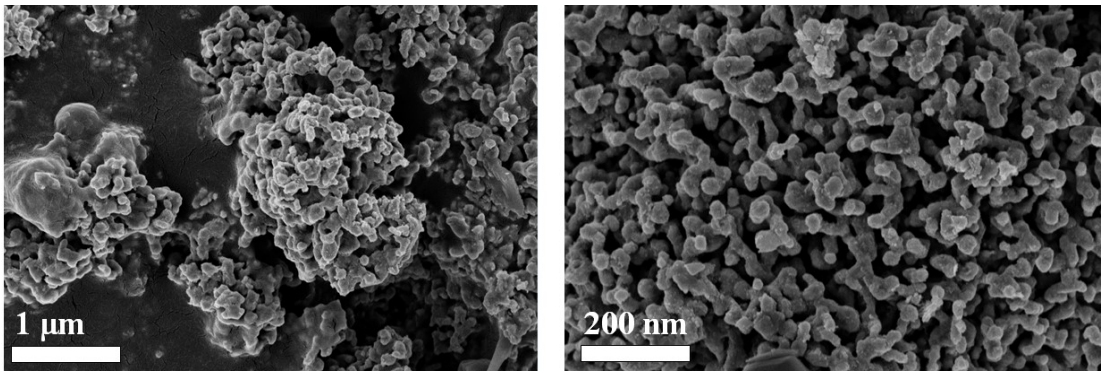

Figure S19. SEM images of NiFeN prepared based on NiFeO precursor.

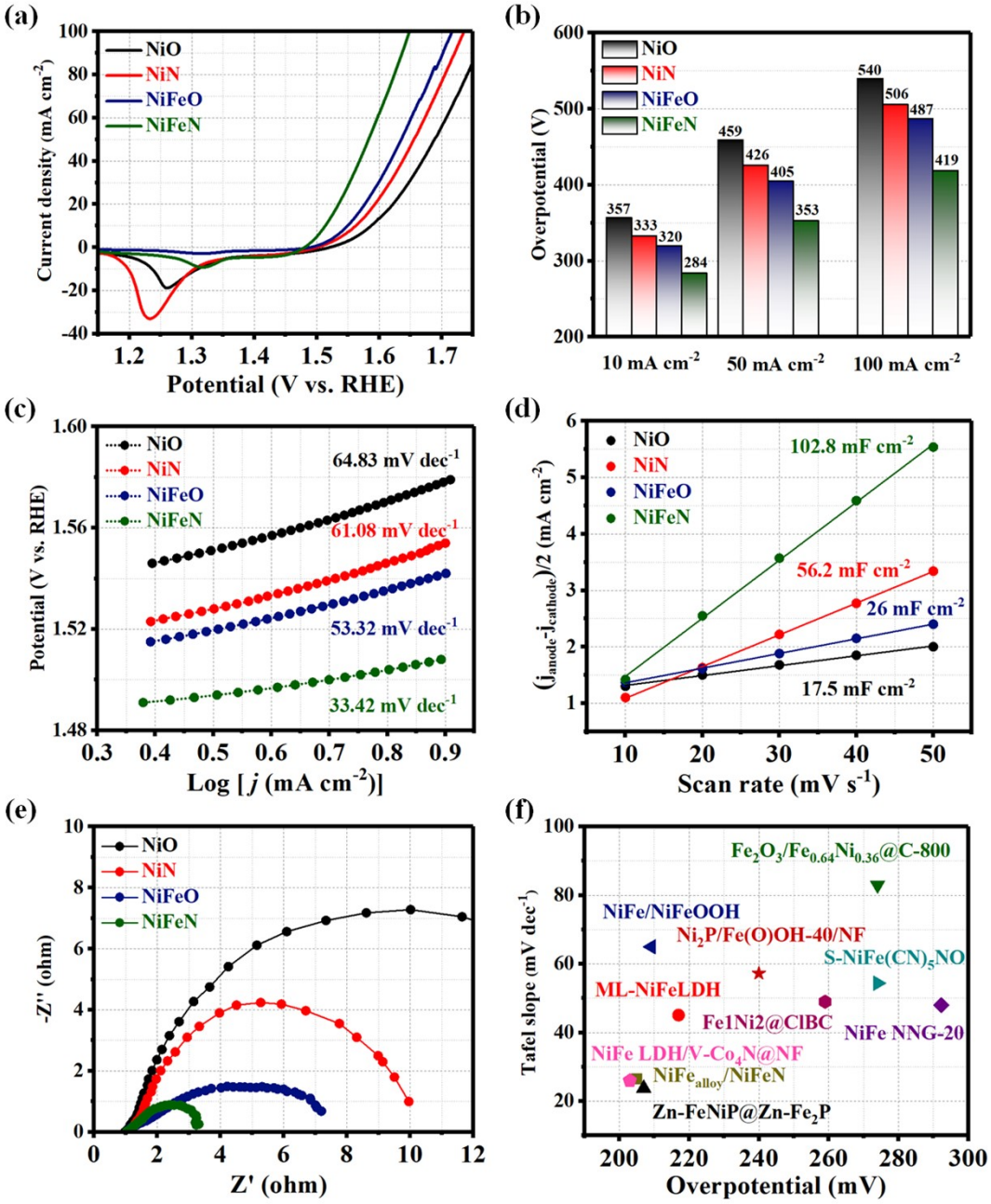

Figure S20. Electrochemical measurement results of different nitrides samples in 1 M KOH: a) LSV curves of OER; b) Overpotential histogram at 10, 50, and 100 mA cm^{-2}; c) Tafel plots; d) The capacitive current at 1.22 V vs RHE as a function of the scan rate; e) Nyquist plots measured at 0.6 V versus Hg/HgO; and f) Comparison of η_{10} overpotential and Tafel slope of $NiFe_{alloy}$/NiFeN with some advanced NiFe-based OER electrocatalysts.

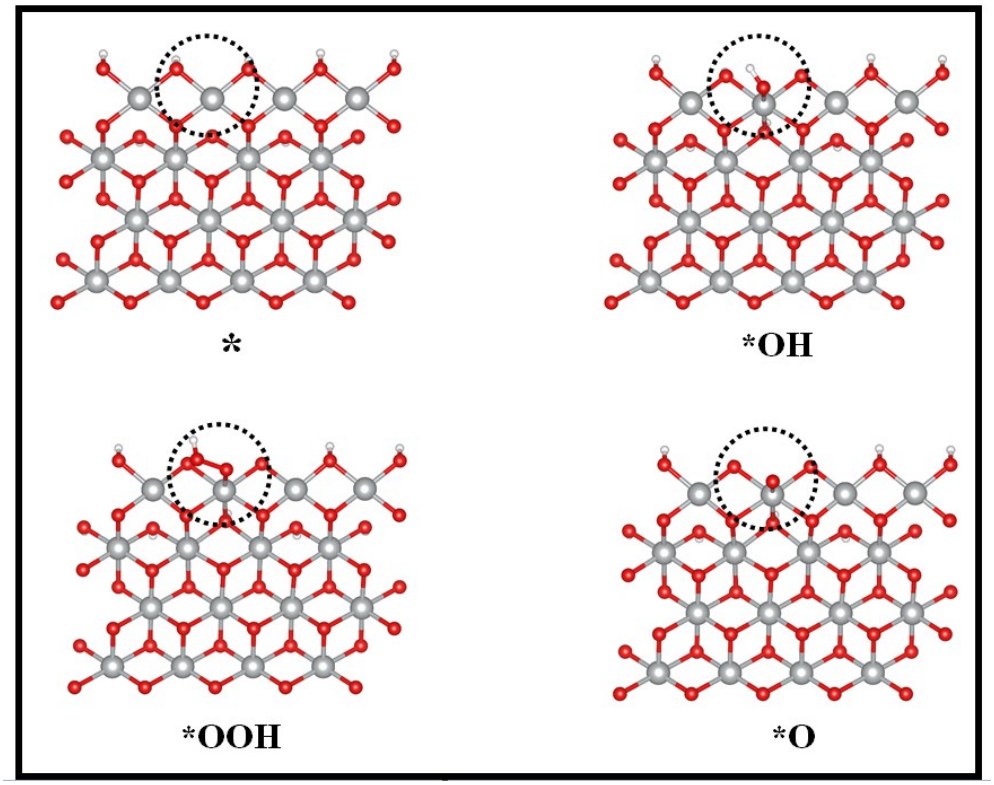

Figure S21. Model structures of the intermediates involved in OER for γ-NiOOH.

Supplementary Tables:

Table S1: The metal elements composition (%) of samples determined by ICP.

Sample	***Ni***	***Fe***
NiFeLDH	56.48	2.23
$NiFe_{alloy}$/NiFeN	84.24	2.08
$NiFe_{alloy}$/NiFeN after OER	78.87	2.46

Table S2: Comparison of OER activity of $NiFe_{alloy}$/NiFeN nanosheets in this work with other reported electrocatalysts in 1 M alkaline solution.

Catalyst	η_{10mA/cm^2} *(mV)*	**Onset potential (mV)**	*Tafel slope (mV dec^{-1})*	*Stability*	*Reference*
$NiFe_{alloy}$/NiFeN	245	220	20.08	120 h at 100 mA cm^{-1}	This work
ML-NiFeLDH	217	205	45.1	20 h at 100 mA cm^{-1}	[1]
NiFeP	265 mV@20 mA	240	58.3	20 h at 10 mA cm^{-1}	[2]
Zn-FeNiP@Zn-Fe_2P	207	195	23.8	50 h at 1.5 V	[3]
Fe_2O_3/$Fe_{0.64}Ni_{0.36}$@C-800	274	270	82.98	15 h at 50 mA cm^{-1}	[4]
NiFe NNG-20	292.3	260	48	20000 s at 50 mA cm^{-1}	[5]
NiFe/NiFeOOH	209.2	175	65	16 h at 10 mA cm^{-1}	[6]
S–$NiFe(CN)_5NO$	274	230	54.4	30 h at 10 mA cm^{-1}	[7]
Ni(Cu)Fe/NF	240 mV@20mA	230	52.8	90 h at 100 mA cm^{-1}	[8]
Fe1Ni2@ClBC	259	240	49	40 h at 10 mA cm^{-1}	[9]
Ni_2P/Fe(O)OH-40/NF	240	220	57.25	20 h at 10 mA cm^{-1}	[10]
NiFe LDH/V–Co_4N@NF	203	180	26	24 h at different current (10:100 mA cm^{-1})	[11]

References

[1] Z. Zheng, D. Wu, G. Chen, N. Zhang, H. Wan, X. Liu, and R. Ma. *Carbon Energy*, 2022, *4*, 901-913.

[2] L. Wei, K. Zhang R. Zhao, L. Zhang, Y. Zhang, S. Yang, and J. Su, *Nano Research*, 2024, 17, 4720–4728.

[3] J. Nie, J. Shi, T. Huang, M. Y. Xie, Z. Y. Ouyang, M. H. Xian, G.F. Huang, H. Wan, W. Hu, and W. Q. Huang, *Adv. Funct. Mater.*, 2024, 4, 2314172.

[4] F. Zhou, M. Gan, D. Yan, X, Chen, and X. Peng, *Small*, 2023, *19*, 2208276.

[5] Z. Lyu, S. Yu, M. Wang, P. Tieu, J. Zhou, Q. Shi, D. Du, Z. Feng, X. Pan, H. Lin, S. Ding, Q. Zhang, and Y. Lin. *Small*, 2024, *20*, 2308278.

[6] D. Peng, C. Hu, X. Luo, J. Huang, Y. Ding, W. Zhou, H. Zhou, Y. Yang, T. Yu, W. Lei, and C. Yuan, *Small*, 2023, *19*, 2205665.

[7] Y. Zhang, X. Shen, C. Song, Z. Ji, and F. H. Du. *J. Mater. Chem. A*, 2023, 11, 8904–8911.

[8] H. Wang, X. Liu, G. Liu, Y. Wang, X. Du, and J. Li. *Chem. Catalysis*, 2023, *3*, 100552.

[9] J. Li, K. Zheng, C. Zhang, L. Jiao, Z. Dong, X. Tao, R. Su, H. Xie, and C. Xu. *Chemical Engineering Journal*, 2023, *462*, 142267.

[10] Y. Xing, S. Liu, Y. Liu, X. Xiao, Y. Li, Z. Wang, Y. Hu, B. Xin, H. Wang, and C. Wang. *Nano Energy*, 2024,*123*, 109402.

[11] S. Zhang, L. Wang, T. Xie, Q. Chen, W. Peng, Y. Li, F. Zhang, and X. Fan. *Journal of Materials Chemistry A*, 2022, *10*, 21523-21530.